The first original version of this manuscript has been submitted on February 28th 2022 for consideration in the peer-reviewed *Solar Energy* journal. Please note that the manuscript has not undergone peer-review yet and has not been formally accepted for publication. Subsequent versions of this manuscript may have slightly different content. Please feel free to contact any of the authors; we welcome feedback.

Photosynthetically Active Radiation Decomposition Models for Agrivoltaic Systems Applications

S. Ma Lu [1, *], S. Zainali[1, *], B. Stridh[1], A. Avelin[1], S. Amaducci[2], M. Colauzzi[2], P.E. Campana[1, *]

1 Mälardalen University, Department of Sustainable Energy Systems, Västerås SE 72123, Sweden

2 Università Cattolica del Sacro Cuore, Department of Sustainable Crop Production, Via Emilia Parmense 84, Piacenza, Italy

Corresponding authors: silvia.ma.lu@mdu.se, sebastian.zainali@mdu.se, pietro.campana@mdu.se

Abstract

Decomposition models of solar irradiance estimate the magnitude of diffuse horizontal irradiance from global horizontal irradiance. These two radiation components are well-known to be essential for the prediction of solar photovoltaic systems performance. In open-field agrivoltaic systems, that is the dual use of land for both agricultural activities and solar power conversion, cultivated crops receive an unequal amount of direct, diffuse and reflected photosynthetically active radiation (PAR) depending on the area they are growing due to the non-homogenously shadings caused by the solar panels installed (above the crops or vertically mounted). It is known that PAR is more efficient for canopy photosynthesis under conditions of diffuse PAR than direct PAR per unit of total PAR. For this reason, it is fundamental to estimate the diffuse PAR component in agrivoltaic systems studies to properly predict the crop yield. Since PAR is the part of electromagnetic radiation in the waveband from 400 to 700 nm that can be used for photosynthesis by the crops, several stand-alone decomposition models of solar irradiance are selected in this study to partition PAR into direct and diffuse. These models are applied and validated in three locations in Sweden: Lanna, Hyltemossa and Norunda, using the coefficients stated on the original publications of the models and locally fitted coefficients. Results showed weaker performances in all stand-alone models for non-locally fitted coefficients (nRMSE ranging from 29% to 95%). However, performances improve with re-parameterization, reaching highest nRMSE of 37.94% in Lanna. YANG2 decomposition model is the best-performing one, reaching lowest nRMSE of 24.31% in Norunda applying re-estimated coefficients. Country level sets of coefficients for the best-performing models, YANG2 and STARKE, are given after parameterization using joined data of the three locations in Sweden. These Sweden-fitted models are tested and showing nRMSE of 25.56% (YANG2) and 28.36% (STARKE). These results can be used to perform estimations of PAR diffuse component in Sweden where measurements are not available, and the overall methodology can be similarly applied to other countries.

Keywords: agrivoltaic, photosynthetically active radiation, decomposition models, diffuse fraction, ICOS

1. Introduction

Solar radiation is the main driver of the planetary energy balance and photosynthesis (Oliphant and Stoy, 2018). For the performance of solar photovoltaic (PV) systems it is necessary to distinguish the magnitude of solar global radiation arriving in its direct beam and diffuse beam forms. Likewise, the different relative levels of these two radiation components result in different irradiance patterns within plant canopies (Norman and Welles, 1983). While for PV systems the total global radiation is the key term, for crops, the analogous term is the photosynthetically active radiation (PAR).

PAR is defined as the part of electromagnetic radiation that can be used as the source of energy for photosynthesis by the plants. PAR is technically defined as radiation in the waveband or spectral range from 400 to 700 nm (McCree, 1972, 1971). It can be expressed either in terms of photosynthetic flux density (PPFD, μmol photons/m^2/s) since photosynthesis is a quantum process, or in terms of photosynthetic radiant flux density (PAR irradiance, W/m^2) more suitable for energy balance studies (Mõttus et al., 2011). As mentioned, PAR reaching the ground surface has two primary incoming streams similar to the incoming total global irradiance: diffuse and direct, which values are essentially affected by the quantity of clouds and aerosols in the atmosphere.

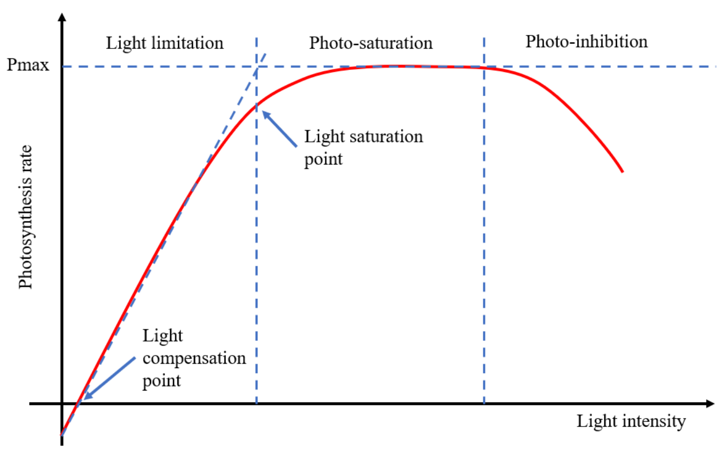

Figure 1. Light-response curve for photosynthesis. The light compensation point is the minimum light intensity at which the plant shows a gain of carbon fixation. Net photosynthesis rate shows a linear rise in response to increased light in light-limitation region. At higher light intensities, saturation occurs (photo-saturation). Under excess of light intensity (photo-inhibition), net photosynthesis declines. Pmax is the maximum rate of photosynthesis. Adapted from (Benedetti et al., 2018; Ferro, 2019)

Photosynthesis in a canopy can be calculated from the amount of light absorbed by the canopy and the light response of the leaves. If the light absorption is averaged over the canopy and over the considered time interval, canopy photosynthesis would be overestimated because of the convex and asymptotic response of photosynthesis (Spitters et al., 1986) (see Figure 1). An important characteristic to be noticed is the fact that direct and diffuse PAR differ in the way they supply energy through plant canopies, hence, affecting canopy photosynthesis processes in a different way than what would take place at the leaf scale (Misson et

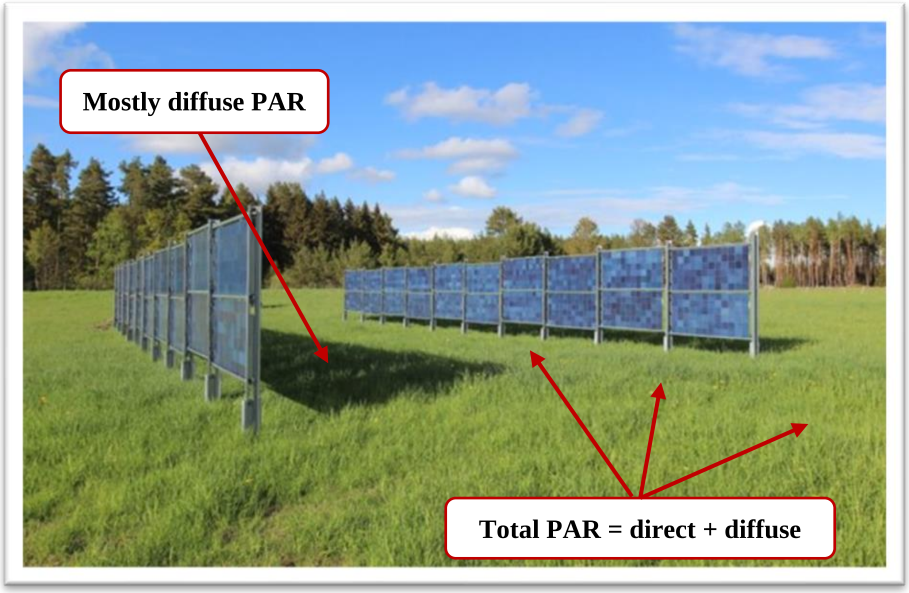

Figure 2. Schematic illustration of the photosynthetically active radiation received at crop level in a vertical bifacial PV system. The picture shows the agrivoltaic system located in Kärrbo Prastgård (Sweden), under the research project “Evaluation of the first agrivoltaic system in Sweden”. Link to the project: (Mälardalens universitet, 2022)

al., 2005). Likewise, diffuse PAR fraction, understood as the ratio of diffuse PAR to the total (direct + diffuse) PAR, in the atmosphere has been positively correlated with higher light-use efficiency and increased CO_2 assimilation in several studies (Alton, 2008; Cheng et al., 2015; Gu et al., 2003, 2002, 1999; Keppel-Aleks and Washenfelder, 2016; Knohl and Baldocchi, 2008; Mercado et al., 2009; Oliphant et al., 2011; Still et al., 2009; Weiss and Norman, 1985), therefore, PAR is more efficient for canopy photosynthesis under conditions of diffuse than direct PAR per unit of total PAR. Within this context, in conventional open-field farming conditions, cultivated crops typically receive total PAR. However, under open-field agrivoltaic systems, that is the dual use of land for both agriculture and solar energy conversion into electricity, cultivated crops receive a combination of direct, diffuse and reflected PAR depending on the shadings caused by the solar panels installed (see Figure 2). Solar panels can be placed in different configurations: above the crops with a specific height or vertically mounted, among others. In all the systems, solar panels produce shadings distributed differently during the day above the crops, hence, the different locations where crops are growing receive different amount of direct, diffuse and reflected PAR. For this reason, in the assessment of agrivoltaic systems and specially crop modelling, it cannot be assumed that all crops receive the same amount of total PAR but an unequal proportion of direct, diffuse and reflected PAR relative to the crop region. Consequently, it is of paramount importance to accurately estimate these different components of PAR and in particular, diffuse PAR.

Diffuse PAR can be measured similarly to measuring diffuse solar irradiation, by employing an array of photodiodes with a unique computer-generated shading pattern to measure incident solar irradiance and using a microprocessor to calculate the global and diffuse components of the radiation that determines the sunshine state (Delta T, 2022; Wood et al., 2003). However, site measurements of the solar irradiation diffuse component are not widely available and less common is to have measurements of diffuse PAR. Instead, diffuse PAR can be estimated by using simple atmospheric radiative transfer models like SPCTRAL2 (Bird and Riordan, 1986) and SMARTS2 (Gueymard, 1995) or by applying less complex models taken from global irradiance diffuse fraction models. Diffuse fraction models have been largely studied and developed for global solar radiation and very few models are actually developed from PAR data sets. Thus, many of these models developed for global solar radiation have been applied to convert the diffuse global solar irradiance fraction into diffuse PAR fraction (Gu et al., 2002; Ren et al., 2018).

Decomposition modeling of solar irradiance is a class of models that estimates diffuse horizontal irradiance (DHI) from global horizontal irradiance (GHI). Decomposition models were mostly developed using hourly data and many are in the form of piecewise polynomial regressions. Likewise, to reduce the model dependency on the diurnal pattern of irradiance, decomposition models are usually developed using the diffuse fraction (i.e., ratio between the diffuse horizontal irradiance and the global horizontal irradiance) $k_d = \frac{\mathrm{DHI}}{\mathrm{GHI}}$, and the clearness index (i.e., the ratio of global solar irradiance measured at ground level (GHI) and its counterpart estimated at the top of the atmosphere or extraterrestrial irradiance on a horizontal plane, $\mathrm{E_{ext}}$ (Liu and Jordan, 1960)) $k_t = \frac{\mathrm{GHI}}{\mathrm{E_{ext}}}$. The models are therefore often visualized using a scatter plot of diffuse fraction against clearness index (Figure 3). However, clearness index is not the only parameter to describe diffuse fraction, from Figure 3 it is clear that one k_t value can be mapped to multiple k_d values.

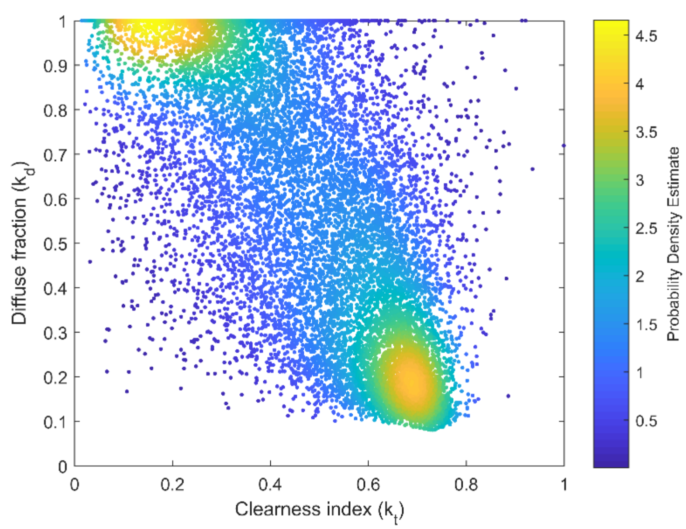

Figure 3. Scatter plot of diffuse fraction vs clearness index. Data extracted from CAMS ("CAMS radiation service," 2021) located in Hyltemossa (Sweden) for years 2015, 2017 and 2018 with a time resolution of 30-min.

Therefore, additional meteorological parameters have been investigated, such as solar zenith angle, apparent solar time, or temperature among others; to estimate diffuse fraction in which the prediction curve is no longer a single-parameter model (line) but a multi-parameter model (hyperplane) (Yang and Boland, 2019).

Several decomposition models of solar global radiation have been proposed during the last decades (Mousavi Maleki et al., 2017) where the performance of the models changes across locations and climates. Gueymard & Ruiz-Arias (2016) analyzed 140 separation models in research-grade stations around the globe and concluded that ENGERER2 was a quasi-universal model. More recent models that appeared after the analysis made by Gueymard & Ruiz-Arias, such as YANG2 (Yang and Boland, 2019) showed even better performance than ENGERER2. Yang & Gueymard (2020) have suggested an Ensemble Model Output Statistics (EMOS) approach to further improve the prediction of diffuse fraction of global radiation based on several decomposition models. In this paper, seven decomposition models, namely: GU, ABREU, ENGERER2, PAULESCU, STARKE, YANG2, and EMOS-based are analyzed to find the most suited model for predicting the diffuse fraction of PAR in Sweden. These models are described in Section 2. As mentioned in Yang & Boland (2019), "*empirical decomposition modeling has been the dominating research focus and practice in solar engineering, therefore it is possible that further improved models will come in the future by fine-tuning them. However, empirical models have limited improvement potential and physically laws governing the relationship between DHI-GHI should instead be emphasized*". Nevertheless, this discussion is out of the scope for the present study.

While empirical models for the estimation of total PAR have been developed in the last decades, for instance the reader is referred to Noriega Gardea et al. (2020) for a review on several estimation methods, few works as far as for the authors' knowledge has been made to compare decomposition models for solar global radiation applied to PAR. For example, the study by Oliphant & Stoy (2018) compared four semiempirical models for partitioning PAR into diffuse and direct beam components. However, only one model was strictly a decomposition model for solar global radiation (ERBS) while the rest were partitioning models formulated already to decompose PAR into direct and diffuse. Previous works have been using global radiation partitioning models into direct and diffuse flux, to similarly develop PAR partitioning models (Gu et al., 1999; Kathilankal et al., 2014; Ren et al., 2018; Spitters et al., 1986), some have roughly estimated diffuse PAR by multiplying PAR total and the diffuse fraction of solar global radiation (Goudriaan and Van Laar, 1994; Leuning et al., 1995). However, the diffuse fraction of global radiation is not equivalent to the diffuse fraction of PAR. For a clear sky, the scattered diffuse component in the PAR wavebands is significantly greater than that in the total global radiation, while under overcast sky both are almost equivalent (Ren et al., 2014; Spitters et al., 1986). To account for this difference, Spitters et al. (1986)

developed a relationship to obtain the diffuse fraction of PAR from the diffuse fraction of global radiation (the reader is referred to section 2.1 for further details regarding this topic). This relationship has been applied previously in other works to determine the fraction of diffuse PAR (Gu et al., 1999; Ren et al., 2018).

The present work aims to find an accurate existing separation model for solar global radiation applicable to PAR, to partition PAR into its diffuse and direct components without having the need to have on-site measurements and only using commonly available inputs. To achieve that, the present work provides a comparison of some of the current best-performing global irradiance decomposition models when applied to PAR diffuse fraction. Furthermore, this study plans to give sets of coefficients fitted for Sweden for the most accurate decomposition models applied to PAR diffuse fraction that would be valuable for the estimation of PAR diffuse component. This will not only benefit agrivoltaic systems assessment but also in related required applications such as simulation models to estimate carbon gain and growth of vegetation (Wang et al., 2006). Finally, this work wishes to emphasize the importance of considering the diffuse component of PAR in agrivoltaic systems due to the shadings that the photovoltaic system can cause to the crops growing underneath and therefore the impact of this variable on the performance and optimization modelling of agrivoltaic systems.

This study is structured as follows. Section 2 describes the six stand-alone decomposition models and the EMOS-based approach selected to be applied to partition PAR. Information on the procurement of the data and the quality control procedure is detailed. Evaluation metrics used for the comparison of the models and the methodology to re-parameterize the models are likewise explained in this section. Section 3 presents the comparison results of the models along with a discussion on which models are more suited for the studied locations. Sets of coefficients for the best-performing models for Sweden are introduced. Section 4 summarizes the outcomes of this study.

2. Methodology

As mentioned in the introduction, the partitioning of PAR into its diffuse and direct components is critical in crop modelling and in agrivoltaic systems due to the shadings created by the solar modules non-homogenously over the plant canopy with spatial and temporal variation. Campana et al. (2021) is one of the first works that incorporates PAR decomposition for determining crop yield in an agrivoltaic system.

2.1. Decomposition models selected

Before introducing the decomposition models selected in this study, to properly take into consideration the difference already explained in the introduction between the diffuse fraction of global radiation and the diffuse fraction of PAR, the relationship developed by Spitters et al. (1986) is employed. Therefore, the approach in this paper is the following: 1) selected decomposition models for solar global radiation are applied to determine diffuse fraction of solar global radiation, 2) the Spitters relationship (Eq.1) is applied to each relevant decomposition model to calculate diffuse fraction of PAR from the diffuse fraction of solar global radiation and, 3) the diffuse component of PAR is obtained from the diffuse fraction of PAR.

$$k_{d\_PAR}^{model} = \frac{PAR_{diffuse}}{PAR_{total}} = \frac{\left[1 + 0.3\left(1 - \left(k_d^{model}\right)^2\right)\right] k_d^{model}}{1 + \left(1 - \left(k_d^{model}\right)^2\right) cos^2(90 - \beta)\, cos^3 \beta} \tag{1}$$

In Eq.1, the superscript model refers to the decomposition model applied to obtain the diffuse fraction of global radiation, k_d, and β is the solar elevation angle [°]. Several models are analyzed and explained in the following section.

A total of seven decomposition models are evaluated in this study. Six stand-alone empirical models are selected and chosen to ensure diversity for the seventh model using EMOS approach (Yang and Gueymard, 2020). Brief model formulations and justification of the selected models are given below. For detailed model formulations and development, the reader is referred to the models' original publications.

1. GU (Gu et al., 1999) referred as reference PAR partitioning model in this study, calculates the diffuse PAR by coupling a decomposition model with two predictors: clearness index and solar elevation angle. The model is based on Reindl et al. (1990) and the Spitters relationship as follows:

$$\frac{DHI}{E_{ext}} = \begin{cases} k_t[1.020 - 0.254k_t + 0.0123 sin\beta], & 0 \le k_t \le 0.3 \\ k_t[1.400 - 1.749k_t + 0.177 sin\beta], & 0.3 < k_t < 0.78 \\ k_t[0.486k_t - 0.182 sin\beta], & k_t \ge 0.78 \end{cases} \tag{2}$$

   Where DHI is the diffuse horizontal irradiance [W/m^2], k_t is the clearness index, E_{ext} is the extraterrestrial radiation [W/m^2] and β is the solar elevation angle [°]. To obtain the diffuse fraction of PAR, Gu et al. (1999) applies a slightly modified Spitters relationship:

$$k_{d\_\mathrm{PAR}}^{\mathrm{GU}} = \frac{\mathrm{PAR_{diffuse}}}{\mathrm{PAR_{total}}} = \frac{[1 + 0.3(1 - q^2)]q}{1 + (1 - q^2)\, cos^2(90 - \beta)\, cos^3 \beta} \tag{3}$$

   Where $q = \left({}^{\mathrm{DHI}}/_{\mathrm{E_{ext}}}\right)/k_t$. For more detailed explanation of the above equations refer to Reindl et al. (1990) and Spitters et al. (1986). This model is chosen as one of the first approaches to partition PAR into its diffuse and direct component based on a decomposition model for global radiation.

2. ENGERER2 (Engerer, 2015) is the highest ranked decomposition model by Gueymard and Ruiz Arias (2016) analysis in performance and it has been often used as a benchmark since then. The

multi-predictor model consists of five parameters developed from a logistic function (main effect) and a cloud-enhancement variable (trend component). Engerer2 is given by:

$$k_d^{\text{Engerer2}} = C + \frac{1 - C}{1 + e^{\beta_0 + \beta_1 k_t + \beta_2 \text{AST} + \beta_3 Z + \beta_4 \Delta k_{tc}}} + \beta_5 k_{de}, \tag{4}$$

$$\Delta k_{tc} = k_{tc} - k_t = \frac{G_{cs}}{E_{ext}} - k_t, \tag{5}$$

$$k_{de} = max\left(0, 1 - \frac{G_{cs}}{\text{GHI}}\right), \tag{6}$$

Where G_{cs} is the clear-sky GHI [W/m^2], Z is the solar zenith angle [°], AST is the apparent solar time [h]. The initial model in 2015 was fitted using Australia data. Four years later, an update using a global parameterization was provided by Bright and Engerer (2019) on the original Engerer2 model. The set of parameters used in this study refer to the global parameterization ones and are as follows: $C = -0.0097539$, $\beta_0 = -5.3169$, $\beta_1 = 8.5084$, $\beta_2 = 0.013241$, $\beta_3 = 0.00743356$, $\beta_4 = -3.0329$, $\beta_5 = 0.56403$. Likewise, Spitters relationship (Eq.1) is applied here to obtain the diffuse PAR fraction from Engerer2 model, $k_{d\_\text{PAR}}^{\text{Engerer2}}$.

3. Paulescu (Paulescu and Blaga, 2016) developed seven linear regression models using different predictors. The models were fitted and tested on datasets from a single location in eastern Europe. PB5 model, as referred by the authors, is the one used in this study. This model uses as predictors clearness index, daily average of clearness index k_{day}, clearness index persistence ψ and the Julian day. The authors of the model emphasized that this model does not include meteorological predictors, thus, not requiring actual measurements. Furthermore, better performance was obtained compared for instance to Reindl (Reindl et al., 1990) and its four predictor model using clearness index, solar elevation angle, air temperature and relative humidity. PB5 model is given by:

$$k_d^{\text{Paulescu}} = \beta_0 + \beta_1^{k_t} k_t + \beta_1^{k_{\text{day}}} k_{\text{day}} + \beta_3 \psi + \beta_4 J + \beta_2^{k_t}(k_t - Bp_1)\theta(k_t - Bp_1) + \beta_2^{k_{day}}\left(k_{\text{day}} - Bp_2\right)\theta\left(k_{\text{day}} - Bp_2\right) \tag{7}$$

This model is segmented after both the clearness index k_t, and the daily average of clearness index k_{day}. The values of k_t and k_{day} at which the surface slope changes are known as breaking points, Bp_1 and Bp_2. θ is the step function:

$$\theta(x) = \begin{cases} 1, & x \geq 0 \\ 0, & x < 0 \end{cases} \tag{8}$$

The daily average of the clearness index is defined as the average values of hourly clearness index in a given day where n is the number of hours within a day:

$$k_{\text{day}} = \frac{1}{n}\sum_{i=1}^{n} k_{t,i} \tag{9}$$

The persistence of the sky conditions ψ is defined as the average of a lag and a lead of the hourly values of the clearness index (Laurent et al, 2010). The regression coefficients fitted for the eastern European site in Romania are used as the reference ones in this study: $\beta_0 = 0.993$, $\beta_1^{k_t} = 0.454$, $\beta_1^{k_{\text{day}}} = -0.063$, $\beta_3 = -0.2$, $\beta_4 = -0.000217$, $\beta_2^{k_t} = -1.796$, $\beta_2^{k_{\text{day}}} = -0.869$, $Bp_1 = 0.248$, $Bp_2 = 0.417$. Spitters relationship (Eq.1) is also applied here to obtain $k_{d\_\text{PAR}}^{\text{PAULESCU}}$ from k_d^{PAULESCU} (Eq.7).

4. STARKE (Starke et al., 2018) is chosen as perhaps one of the most accurate of logistic-function-based separation models which has been demonstrated to outperform ENGERER2 at several locations in Australia and Brazil. Starke decomposition model is given by:

$$k_d^{\text{STARKE}} = \begin{cases} \dfrac{1}{1 + e^{\beta_7 + \beta_8 k_t + \beta_9 AST + \beta_{10} Z + \beta_{11} K_T + \beta_{12}\psi + \frac{\beta_{13} G_{cs}}{277.78}}}, & k_{CSI} \geq 1.05 \text{ and } k_t > 0.65; \\ \dfrac{1}{1 + e^{\beta_0 + \beta_1 k_t + \beta_2 AST + \beta_3 Z + \beta_4 K_T + \beta_5 \psi + \frac{\beta_6 G_{cs}}{277.78}}}, & \text{otherwise} \end{cases} \tag{10}$$

$$K_T = \frac{\sum_{n=1}^{24} \text{GHI}_n}{\sum_{n=1}^{24} \text{E}_{\text{ext}_n}} \tag{11}$$

Where K_T is the daily clearness index (Eq.11), ψ predictor is defined, in this work, as the three-point moving average of clearness index since higher performance is obtained; ψ used in the study by Starke et al., (2018) was instead defined as average of both lag and lead of clearness index, k_{CSI} is the clear-sky index understood as the ratio between GHI and G_{cs}.

Well analyzed by Yang & Boland (2019), STARKE model although having superior performance than ENGERER2, it has seven parameters and two of them, K_T and ψ are smoothing parameters that depend on future values of k_t. Thus, if a real-time predictor is to provide the same smoothing effect it would probably outperform STARKE. The original published set of coefficients also used in this work are: $\beta_0 = -6.70407$, $\beta_1 = 6.99137$, $\beta_2 = -0.00048$, $\beta_3 = 0.03839$, $\beta_4 = 3.36003$, $\beta_5 = 1.97891$, $\beta_6 = -0.96758$, $\beta_7 = 0.15623$, $\beta_8 = -4.21938$, $\beta_9 = -0.00207$, $\beta_{10} = -0.06604$, $\beta_{11} = 2.12613$, $\beta_{12} = 2.56515$, $\beta_{13} = 1.62075$.

Spitters relationship (Eq.11) is applied to the values of k_d^{STARKE} from (Eq.10) to finally obtain $k_{d\_\text{PAR}}^{\text{STARKE}}$.

5. ABREU (Abreu et al., 2019) model is chosen to exemplify the single predictor decomposition model where many early researchers used clearness index as sole predictor for diffuse fraction. The model

is developed from 1-min data, however in this study, 30-min data is used instead since the measured data falls in this temporal range. ABREU model is given by:

$$k_d^{\mathrm{ABREU}} = \{1 + [A(k_t - 0.5)^2 + B(k_t - 0.5) + 1]^{-n}\}^{-\frac{1}{n}} \tag{12}$$

Where A, B and n are fitting parameters. Abreu used data from 48 worldwide radiometric stations belonging to different climate zones and proposes a set of parameters for each climate zone: Arid (AR), High Albedo (HA), Temperate (TM) and Tropical (TR) (Table 1). To obtain the diffuse PAR fraction applying Abreu model, $k_{d\_\mathrm{PAR}}^{\mathrm{ABREU}}$, the authors of this paper also applied Spitters relationship (Eq.1) from the diffuse fraction of global radiation obtained above in Eq.12.

Table 1. Reference parameters fitted for the model developed by Abreu et al., (2019) according to the different climate zones: Arid (AR), High Albedo (HA), Temperate (TM) and Tropical (TR).

Parameters	**Climate Zone**			
	AR	**HA**	**TM**	**TR**
A	11.39	7.83	10.79	11.59
B	-6.25	-4.59	-5.87	-6.14
n	1.86	3.25	2.24	1.87

6. YANG2 (Yang and Boland, 2019) model is selected since it appears to be the best performing stand-alone decomposition model to date. The model is developed deriving out of ENGERER2 and STARKE models and is given by:

$$k_d^{\mathrm{YANG2}} = C + \frac{1 - C}{1 + e^{\beta_0 + \beta_1 k_t + \beta_2 \mathrm{AST} + \beta_3 Z + \beta_4 \Delta k_{tc} + \beta_6 k_d^{(s)}}} + \beta_5 k_{de}, \tag{13}$$

Where $k_d^{(s)}$ is the satellite-derived diffuse fraction. The choice of this predictor is thought to be opportune by the authors of the model due to the worldwide availability of physically based satellite-derived irradiance data, the inclusion of physics aspects in decomposition modeling and it provides the smoothing effect that STARKE model has without relying on future values. The YANG2 model coefficients have been fitted to seven SURFRAD stations from the United States of America, being $C = 0.0361$, $\beta_0 = -0.5744$, $\beta_1 = 4.3184$, $\beta_2 = -0.0011$, $\beta_3 = 0.0004$, $\beta_4 = -4.7952$, $\beta_5 = 1.4414$, $\beta_6 = -2.8396$ and these are used as reference ones in this study. Here, the values of k_d^{YANG2} (Eq.13) are also used in the Spitters relationship (Eq.1) to get $k_{d\_\mathrm{PAR}}^{\mathrm{YANG2}}$ estimates.

7. Ensemble model output statistics or EMOS based decomposition model is a parametric post-processing framework to make probabilistic predictions, as opposed to deterministic predictions that the previously described stand-alone decomposition models are. EMOS takes the diffuse fractions of global radiation estimated by an ensemble of existing models and outputs a predictive

distribution with parameters optimized by maximum likelihood estimation (MLE). Yang & Gueymard (2020) found out that EMOS post-processed predictions for several locations in the USA and Europe gave better results than the best stand-alone model YANG2. For further details on EMOS approach modelling procedure, the reader is referred to Yang & Gueymard (2020) and Gneiting et al. (2005).

Briefly, for sample $i \in [1, 2, \dots, n]$ and m decomposition models, $X_{i1}, \dots, X_{im}$, are the decomposition models estimates. Being Y_i the observations, the predictive distribution of Y_i should take the form of a multiple linear regression as suggested by Gneiting et al. (2005):

$$\widehat{Y}_i \sim N\left(b_1 X_{i1} + \cdots + b_m X_{im}, cS_i^2\right), \tag{14}$$

$\widehat{Y}_i$ is a normal distribution with mean $b_1 X_{i1} + \cdots + b_m X_{im}$ and variance cS_i^2, where c is a scaling constant and S_i^2 is the ensemble variance given by:

$$S_i^2 = \frac{1}{m-1}\left[\sum_{k=1}^{m} X_{ik}^2 - \frac{1}{m}\left(\sum_{k=1}^{m} X_{ik}\right)^2\right]. \tag{15}$$

To ensure that the EMOS estimate is in the same range as the decomposition models estimates, an equality constraint $\sum_{k=1}^{m} b_m = 1$ to the EMOS model parameters, namely $b_1, \dots, b_m$ is necessary. To ensure positivity of the variance, an inequality constraint, $c > 0$, is applied. The EMOS model parameters and c can be estimated by maximizing the log-likelihood in:

$$\ell_n(b_1, \dots, b_m, c) = log\mathcal{L}_n(b_1, \dots, b_m, c), \tag{15}$$

where the sample likelihood function of Eq.15 is:

$$\mathcal{L}_n(b_1, \dots, b_m, c) = \prod_{i=1}^{n} f(Y_i; b_1, \dots, b_m, c)\,, \tag{16}$$

and f is a normal probability density function (PDF):

$$f(Y_i; b_1, \dots, b_m, c) = \frac{1}{\left(2\pi c S_i^2\right)^{\frac{1}{2}}} exp\left\{-\frac{[Y_i - (b_1 X_{i1} + \cdots + b_m X_{im})]^2}{2cS_i^2}\right\}. \tag{17}$$

Finally, with the estimated parameters, i.e., $\hat{b}_1, \dots, \hat{b}_m$, $\hat{c}$, when a new set of decomposition model's predictions take place, $X_{*1}, \dots, X_{*m}$, the mean and variance of the EMOS estimate are respectively:

$$\mathbb{E}\left(\widehat{Y}_*\right) = \hat{b}_1 X_{*1} + \cdots + \hat{b}_m X_{*m}, \tag{18}$$

$$\mathbb{V}\left(\widehat{Y}_*\right) = \hat{c} S_*^2. \tag{19}$$

In this study, a similar approach as Yang & Gueymard (2020) is applied for the estimation of the diffuse fractions of PAR, $k_{d\_\mathrm{PAR}}^{\mathrm{model}}$, via the six decomposition models described previously to obtain $k_{d\_\mathrm{PAR}}^{\mathrm{EMOS}}$.

2.2. Data

The dataset used for testing and validating the decomposition models with their reference parameters (i.e., extracted from the original publications of each model) and the dataset for training the models (i.e., to find fitting coefficients to each model) to the studied sites consist of multiple-year measurements of total PAR and diffuse PAR among other variables from the Integrated Carbon Observation System in Sweden ("ICOS Sweden," 2021) network. Three locations in Sweden with available measured data were selected: Lanna, Hyltemossa and Norunda. as presented in Figure 4. The data refers to three years for each station at a time resolution of 30 minutes including global horizontal irradiance, PAR total and PAR diffuse. The measurements of PAR from ICOS stations are in units of flux density as a quantum process (PPFD), thus, the following conversion factor is applied when needed, $1\ \mathrm{W/m^2} \approx 4.6\ \mathrm{\mu mol/m^2}/s$ (Langhans et al., 1997). The data for each location is divided in two sets: the training set with two years of data used to determine the fitting parameters of the chosen models for the site; and the validation or testing set with one year of data used to both test the models with their original parameters and with the newly fitted ones for the selected location. A detailed description of the considered sites and the annual data used in this study is presented in Table 2. The climate area is chosen according to the re-analyzed Köppen-Geiger map (Kottek et al., 2006; Rubel et al., 2017).

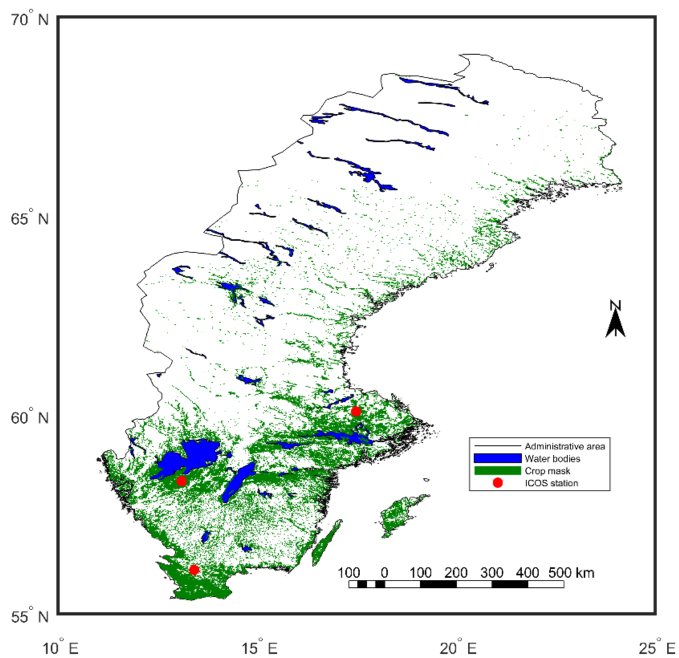

Figure 4. Location of the ICOS-Sweden stations included in the analysis.

Table 2. Information on the data of ICOS-Sweden stations studied. TM (Temperate). Last column indicates the number of validation points "samples" at each location applied for the training set and the testing set respectively.

Station	Latitude (ºN)	Longitude (ºE)	Elevation (m)	Climate Area	Data period	Samples training/ testing
Lanna	58º20'	13º06'	75	TM	2017-2019	14239/ 6423
Hyltemossa	56º06'	13º25'	115	TM	2015, 2017- 2018	12016/ 5468
Norunda	60º05'	17º29'	46	TM	2016-2018	11220/ 5339

2.2.1. Other data

The methodology to extract other input variables that are needed for the decomposition models and that are not given in the ICOS data sets is explained in this section.

Extraterrestrial radiation on a horizontal plane needed for computing clearness index is calculated, as explained in Duffie & Beckman (2013), through the solar constant defined by Gueymard (2018), $SC = 1361.1\ \mathrm{W/m^2}$, the Earth's orbit eccentricity correction factor defined by Spencer's equation (Spencer, J. W, 1971) and the zenith angle. The zenith angle is calculated through the solar elevation and the latter is obtained using the algorithm for solar position developed by Koblick (2021). Moreover, to account for the atmospheric refraction effects, the model from the ESRL Global Monitoring Laboratory (US Department of Commerce, 2021) is applied to correct the solar elevation angle. The clear-sky global horizontal irradiance needed for ENGERER2, STARKE and YANG2 is determined through the model developed by Robledo & Soler (2000). Furthermore, YANG2 requires the satellite-derived diffuse fraction. For European sites, the Copernicus Atmosphere Monitoring Service radiation service ("CAMS radiation service," 2021; Gschwind et al., 2019; Lefèvre et al., 2013; Qu et al., 2017) developed by the European Centre for Medium-Range Weather Forecasts has 15-min satellite-derived GHI and DHI data since 2004 and a spatial coverage of -66º to 66º in both latitudes and longitudes. The satellite-derived data is downloaded to match the spatial and temporal characteristics of the measured ICOS data.

2.2.2. Quality control of observation data

Observations with poor quality may offset the parameter values of estimation models affecting the quality of the generated PAR diffuse fraction and thus PAR diffuse estimation. Hence, after downloading the data from ICOS network, several quality control (QC) filters are applied to guarantee only the highest-quality data points are used during the comparison, validation, and further establishment of new fitting parameters of all the models. Since there is currently no ideal or widely accepted procedure for the optimal QC of irradiance data (Gueymard and Ruiz-Arias, 2016) neither there is a consensus for QC of measured PAR data (e.g., the reader is referred to the following publications for broad diversity of quality filters regarding measured PAR data (Cruse et al., 2015; Hu et al., 2007; Jacovides et al., 2010, 2003; Kathilankal et al., 2014; Laccio et al., 2021; Oliphant and Stoy, 2018; Ren et al., 2018; S et al., 2017; Tsubo and Walker, 2005; Wang et al., 2006)), in the present work, the quality checks are made according to the following criteria:

1. $\mathrm{GHI} \leq 1.2\mathrm{E_{ext}}$, QC proposed by the European Commission's Daylight project (Kathilankal et al., 2014).
2. $\mathrm{GHI} > 5\ \mathrm{W/m^2}$, QC proposed by the European Commission's Daylight project (Kathilankal et al., 2014).
3. $Z < 85°$, (Gueymard and Ruiz-Arias, 2016) to avoid cosine response issues.
4. $\mathrm{PAR_{total}} < \mathrm{PAR_{ext}}$, (Hu et al., 2007) and the extraterrestrial PAR is derived from the extraterrestrial radiation, $\mathrm{E_{ext}}$ (explained in Section 2.2.1) with a widely accepted fraction of 0.39 (Cebula et al., 1996; Gueymard, 2004; Smith and Gottlieb, 1974), i.e. $\mathrm{PAR_{ext}} = \mathrm{E_{ext}} \times 0.39\ [\mathrm{W/m^2}]$.
5. $0.28 < \frac{\mathrm{PAR_{total}}}{\mathrm{GHI}} < 0.61$, (Hu et al., 2007; S et al., 2017).
6. $\text{Relative Humidity} < 100\%$, otherwise measurement accuracy might be affected by water droplets formed on the sensor (Kathilankal et al., 2014).
7. $\text{Precipitation} < 2.5\ \mathrm{mm}$, for half-hourly values otherwise measurement accuracy might be affected by water droplets formed on the sensor (Kathilankal et al., 2014).

Those measured data points not respecting the above conditions were rejected and not considered for the analysis. Furthermore, k_{d_PAR} values higher than 1 and lower than 0 are also removed since measurements of diffuse PAR irradiance higher than total PAR irradiance are very questionable.

2.3. Statistical indicators for models' assessment

For PAR measurement, there are no standard evaluation metrics accepted so far (Nwokolo, 2018). In this study, all the six stand-alone models and the EMOS reviewed in section 2.1 above are evaluated using three commonly applied error metrics described below taking the measured values from the ICOS stations as observations. It is noted that although all decomposition models estimate first k_d (diffuse fraction of global solar radiation) and then apply Spitters relationship to obtain k_{d_PAR} (diffuse fraction of PAR), with the exception of GU and EMOS models that already estimates k_{d_PAR}, the errors are computed based on PAR diffuse component ($\mathrm{PAR_{diff}}$), i.e., $\mathrm{PAR_{diff}} = k_{d\_\mathrm{PAR}} \times \mathrm{PAR_{total}}$. These three statistical indicators are the normalized mean bias error (nMBE), normalized root mean square error (nRMSE), and the coefficient of determination (R^2).

$$\mathrm{nMBE} = \frac{\frac{1}{n}\sum_{t=1}^{n}\left[\widehat{\mathrm{PAR}}_{\mathrm{diff}}(t) - \mathrm{PAR}_{\mathrm{diff}}(t)\right]}{\frac{1}{n}\sum_{t=1}^{n}\mathrm{PAR}_{\mathrm{diff}}(t)} \times 100, \tag{20}$$

$$\mathrm{nRMSE} = \frac{\sqrt{\frac{1}{n}\sum_{t=1}^{n}\left[\widehat{\mathrm{PAR}}_{\mathrm{diff}}(t) - PAR_{\mathrm{diff}}(t)\right]^2}}{\frac{1}{n}\sum_{t=1}^{n}\mathrm{PAR}_{\mathrm{diff}}(t)} \times 100, \tag{21}$$

$$\mathrm{R}^2 = 1 - \frac{\sum_{t=1}^{n}\left[\mathrm{PAR}_{\mathrm{diff}}(t) - \widehat{\mathrm{PAR}}_{\mathrm{diff}}(t)\right]^2}{\sum_{t=1}^{n}\left(\mathrm{PAR}_{\mathrm{diff}}(t) - \frac{1}{n}\sum_{t=1}^{n}\mathrm{PAR}_{\mathrm{diff}}(t)\right)^2} \tag{22}$$

Where n for each station is the number of validation (testing) points used and it is listed in the last column of Table 2. For nMBE, values closer to zero indicate a better model accuracy, for nRMSE lower values are preferred whereas for R^2, values closer to one represent better model accuracy.

2.4. Re-parameterization of coefficients

Since one of the targets of this study is to provide accurate estimations of diffuse PAR for Sweden based on decomposition models, it is not enough to select the best model and apply their originally fitted coefficients since many of these models are suited for data from locations with very different weather and climate than Sweden. Hence, a re-parameterization to find fitted coefficients for the locations studied is deemed to not only improve the overall performances of the several models but also assist in the decision-making of which of the decomposition models is the most suitable for northern latitudes.

The training data as described in Table 2 for the three studied locations is used to estimate the new set of coefficients for each of the models. The coefficients are estimated via a nonlinear optimization solver-based approach from the programming and numeric computing platform MATLAB, specifically `fmincon` solver ("MathWorks," 2021) is employed. The target function or fitness function to minimize for the stand-alone models is chosen to be the mean absolute error (MAE) of the diffuse fraction of PAR, i.e., the ratio between the diffuse PAR and total PAR. For the EMOS approach, the target function in this case is the ignorance score (Eq.24), as explained by Gneiting et al. (2005) in their publication, the maximum likelihood estimation is equivalent to minimizing the ignorance score for the training data.

$$\mathrm{MAE} = \frac{1}{n}\sum_{i=1}^{n}\left|\hat{Y}_i - Y_i\right|, \tag{23}$$

$$\mathrm{IGN} = \frac{1}{n}\sum_{i=1}^{n}\left[\frac{1}{2}ln\left(2\pi c S_i^2\right) + \frac{[Y_i - (b_1X_{i1} + \cdots + b_mX_{im})]^2}{2cS_i^2}\right], \tag{24}$$

Where $Y_i = k_{d\_\mathrm{PAR_i}}^{\mathrm{measured}}$, $\hat{Y}_i = k_{d\_\mathrm{PAR_i}}^{\mathrm{model}}$ and n for each station is the number of training points used and it is listed in the last column of Table 2.

3. Results and discussion

Brief analysis on the spatial and temporal distribution of measured PAR and GHI ratio is given for the three locations studied in this section. The performance comparison of the decomposition models analyzed for the locations studied both using the original coefficients as well as reparametrized coefficients are presented in this section following a discussion. The most accurate models are ranked and the sets of coefficients applicable for Sweden at country level are proposed for these.

3.1. PAR/GHI distribution

PAR/GHI ratio is known to show spatial and temporal variability (Hu et al., 2007) although a constant ratio is frequently assumed (Ferrera-Cobos et al., 2020). Figure 5 shows the mean monthly variation of the PAR/GHI ratio of the selected years in the studied locations. Effectively, there are variability between the locations, the months, and the years. In Noriega Gardea et al. (2020) review, this ratio generally exhibits its maximum values during the summer months and the lowest in the winter months. However, there are exceptions to this rule (Yu and Guo, 2016), as it can be seen in Figure 5, where the trend for some years shows lower fractions in the summer months and higher ones in winter months. Likewise, PAR/GHI

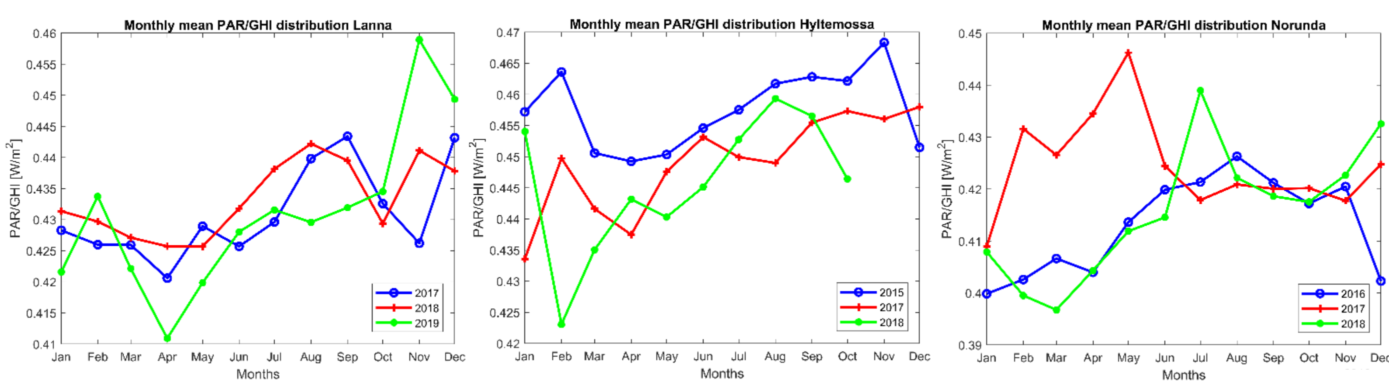

Figure 5. Temporal distribution of PAR/GHI ratio in Lanna (left), Hyltemossa (center) and Norunda (right) for the analyzed years. Values are monthly averages. Note that Hyltemossa lacks data from November and December 2018.

displays its highest variability in autumn and winter months for most of the locations and years, which agrees with the analysis performed by Noriega Gardea et al. (2020). The results from a study conducted by Xia et al. (2008) shows that the monthly values for the PAR/GHI ratio in temperate areas fall in the range of 1.87 to 2.08 mol/MJ (i.e., 0.40 to 0.45 using the conversion factor by Langhans et al. (1997)), which is very similar to the results displayed in Figure 5 (all values fall between 0.39 and 0.47).

3.2. Decomposition models comparison

Solar radiation decomposition modeling is useful when on-site diffuse measurements are not available or incorrect. The main goal for decomposition models is to predict DHI accurately at any arbitrary locations, and in the case of this study, to predict accurately PAR diffuse component.

Table 3. The nRMSE [%], nMBE [%] and R^2 of 6 stand-alone decomposition models (using original coefficients) validated at 3 ICOS-Sweden stations over a period of 1 year (Lanna 2019, Hyltemossa 2018, Norunda 2018). The errors are computed between the predicted and measured 30-min PAR diffuse values. For EMOS, data from the two first years of each location described in Table 2 are used for parameter estimation, the errors are reported for the period of 1 year (same year as for the other models). Boldface denotes the best-performing model in a row.

Station	**GU**	**ABREU (TM)**	**ENGERER2 (-)**	**PAULESCU (Romania)**	**STARKE (Brazil)**	**YANG2 (USA)**	**EMOS**
				nRMSE (%)			
Lanna	36.53	36.82	42.51	49.57	32.96	32.19	**28.42**
Hyltemossa	37.8	37.42	42.54	95.32	37.47	33.96	**31.5**
Norunda	33.03	31.29	33.2	30.91	30.44	29.65	**26.6**
				nMBE (%)			
Lanna	**-0.12**	0.77	-4.22	-16.6	2.83	7.43	2.34
Hyltemossa	15.68	17.18	18.53	13.16	16.65	**11.53**	13.76
Norunda	3.95	7.04	**0.47**	-4.89	6.82	7.42	5.68
				R^2			
Lanna	0.7	0.69	0.59	0.44	0.75	0.76	**0.82**
Hyltemossa	0.61	0.65	0.55	-1.35	0.65	0.7	**0.74**
Norunda	0.71	0.74	0.71	0.73	0.74	0.77	**0.8**

The error metrics for PAR diffuse component obtained for the three investigated locations using the selected seven models with their original parameters are shown in Table 3. By examining the results, one-parameter model ABREU and two-parameter model GU are insufficient to model the non-injective diffuse PAR component, this is also observable in Figure 6. For the other more complex models, surprisingly, ENGERER2 (top-ranked model by Gueymard and Ruiz Arias (2016)) using global parameterization coefficients found by Bright and Engerer (2019) performs poorly particularly for Lanna (nRMSE of 42.51%) and Hyltemossa (nRMSE 42.54%), meaning that these globally fitted parameters are not representative for Swedish environments. PAULESCU also performs very poorly for Lanna (nRMSE of 49.57%) and in particular for Hyltemossa (nRMSE of 95.32%), since the model is based on a linear-regression technique, is it known that coefficients are highly subjective to fitting data. STARKE and YANG2, more recent models that claimed in their publications their superiority to ENGERER2, they are indeed proved in this study as well, being YANG2 the best performing stand-alone model for all three locations in terms of nRMSE and R^2.

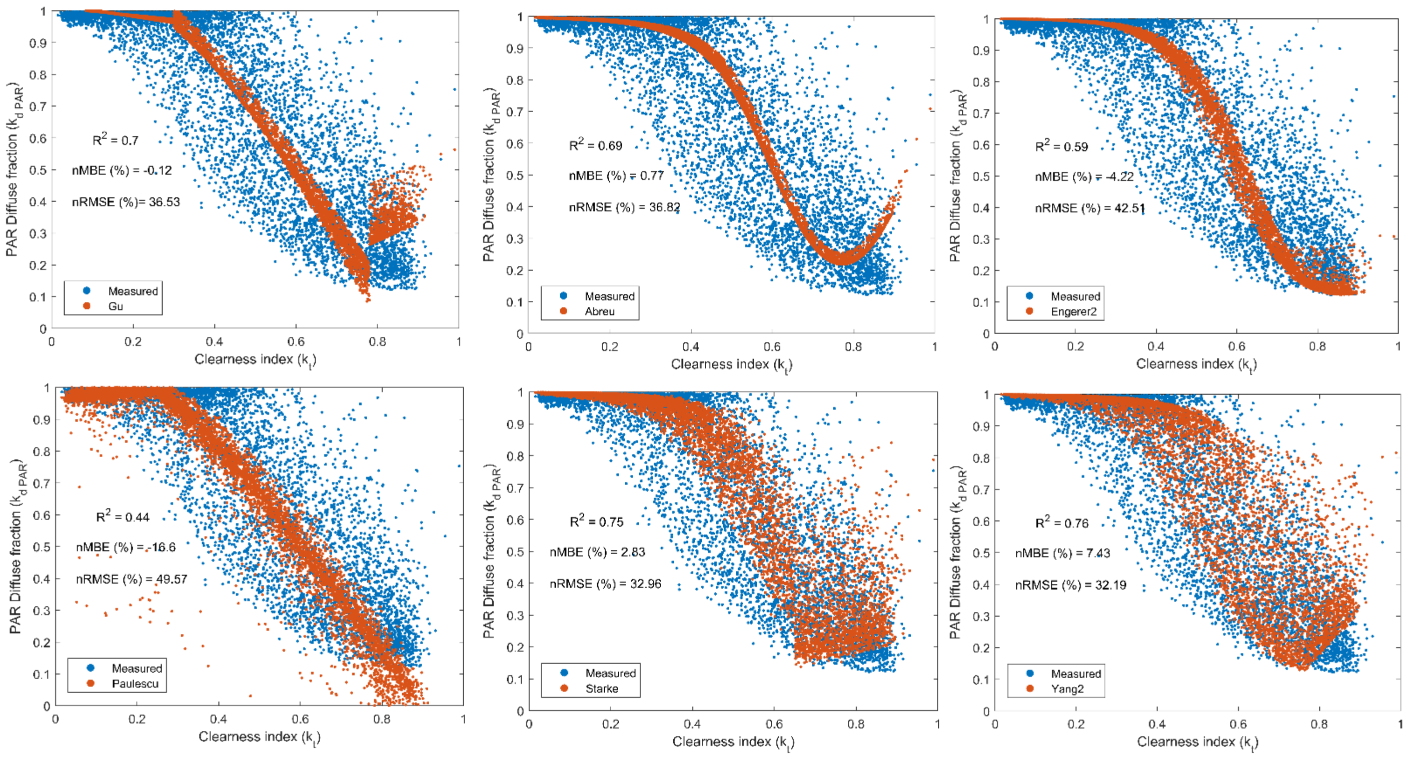

Figure 6. Diffuse PAR fraction data plotted against clearness index for the Lanna station, overlaid with the results of six stand-alone decomposition models using their original coefficients. The total number of data points in each plot is the testing data sample listed in Table 2.

Since EMOS model requires parameter fitting, the training data described in section 2.2 is firstly used for fitting the parameters. Afterwards, to make the EMOS model comparable to the rest, the same testing data is applied to compute the reported errors in Table 3. Based on nRMSE and R^2, EMOS performs slightly better than the best stand-alone model (YANG2) for all the locations. Table 4 shows the estimated mixing weights of the 6 stand-alone models. As expected, the best performing stand-alone model, YANG2 contributes significantly towards the mean of the final EMOS estimate. Surprisingly, GU model has also higher contribution which could be attributed to the poor performance of the other models for Swedish locations and the low nMBE of the model. Hence, Table 4 emphasizes the models low applicability to the locations studied and the need of locally fitted parameters for improved accuracy.

Table 4. Station-specific EMOS parameters estimated using 30-min data from ICOS-Sweden stations (Lanna 2017-2018, Hyltemossa 2015 and 2017, Norunda 2016-2017). Parameters $\hat{b}^{\text{GU}}, \cdots, \hat{b}^{\text{YANG2}}$ are the estimated mixing weights for the 6 component models respectively, whereas $\hat{c}$ is the estimated amount of scaling for the ensemble variance.

Station	$\hat{b}^{\text{GU}}$	$\hat{b}^{\text{ABREU}}$	$\hat{b}^{\text{ENGERER2}}$	$\hat{b}^{\text{PAULESCU}}$	$\hat{b}^{\text{STARKE}}$	$\hat{b}^{\text{YANG2}}$	$\hat{c}$
Lanna	0.19	0.00	0.00	0.11	0.21	0.49	0.60
Hyltemossa	0.50	0.00	0.00	0.01	0.00	0.49	0.60
Norunda	0.37	0.00	0.00	0.06	0.23	0.34	0.06

Table 5. The nRMSE [%], nMBE [%] and R^2 of 6 stand-alone decomposition models (using locally fitted coefficients except GU) validated at 3 ICOS-Sweden stations over a period of 1 year (Lanna 2019, Hyltemossa 2018, Norunda 2018). The errors are computed between the predicted and measured 30-min PAR diffuse values. For EMOS, data from the two first years of each location described in Table 2 are used for parameter estimation and by using the newly fitted coefficients on the stand-alone models (except GU), the errors are reported for the period of 1 year (same year as for the other models). Boldface denotes the best-performing model in a row.

Station	**GU**	**ABREU (local)**	**ENGERER2 (local)**	**PAULESCU (local)**	**STARKE (local)**	**YANG2 (local)**	**EMOS**
				nRMSE (%)			
Lanna	36.53	36.72	33.72	37.94	28.54	26.23	**25.67**
Hyltemossa	37.8	31.27	29.51	29.57	25.83	24.83	**24.35**
Norunda	33.03	30.4	29.29	27.68	25.73	24.31	**23.96**
				nMBE (%)			
Lanna	**-0.12**	-2.66	-3.3	-9.78	-4.12	-2.56	-3.32
Hyltemossa	15.68	4.4	-2.13	**-0.33**	-3.82	-1.56	-1.96
Norunda	3.95	2.38	-1.23	**0.07**	-5.63	-2.23	-3.51
				R^2			
Lanna	0.7	0.69	0.74	0.67	0.81	0.84	**0.85**
Hyltemossa	0.61	0.73	0.76	0.76	0.82	0.83	**0.84**
Norunda	0.71	0.75	0.77	0.78	0.81	**0.84**	**0.84**

Sets of re-estimated coefficients using the training data sets described in section 2.2 for each location are likewise validated with the same testing data sets as in the previous case. The new validation results for PAR diffuse component prediction are shown in Table *5*. For all models and locations, except GU that has not been re-parameterized since it was taken in this study as the reference PAR decomposition model, the newly estimated coefficients locally fitted give better performance when compared to the previous results in Table 3. However, the overall trend between the models is similar as explained in the case of non-locally fitted parameters: YANG2 is still the best stand-alone performing model in terms of nRMSE and R^2 followed closely by STARKE, and ENGERER2 is in the third place. PAULESCU performance although showing great improvement with locally fitted parameters compared to non-locally fitted ones, the model still cannot explain the behavior of k_{d_PAR} to k_t as well as the other more performing models (see Figure 7). Again, EMOS, attempting to optimize predictions by leveraging a collection of stand-alone models, outperforms all the other models. As contrary to the previous results, the new weighting estimates of the models shown in Table 6 are more in accordance with the literature and it demonstrates clearly the significant high contribution of YANG2 and STARKE suggesting that YANG2 and STARKE are already highly accurate stand-alone models.

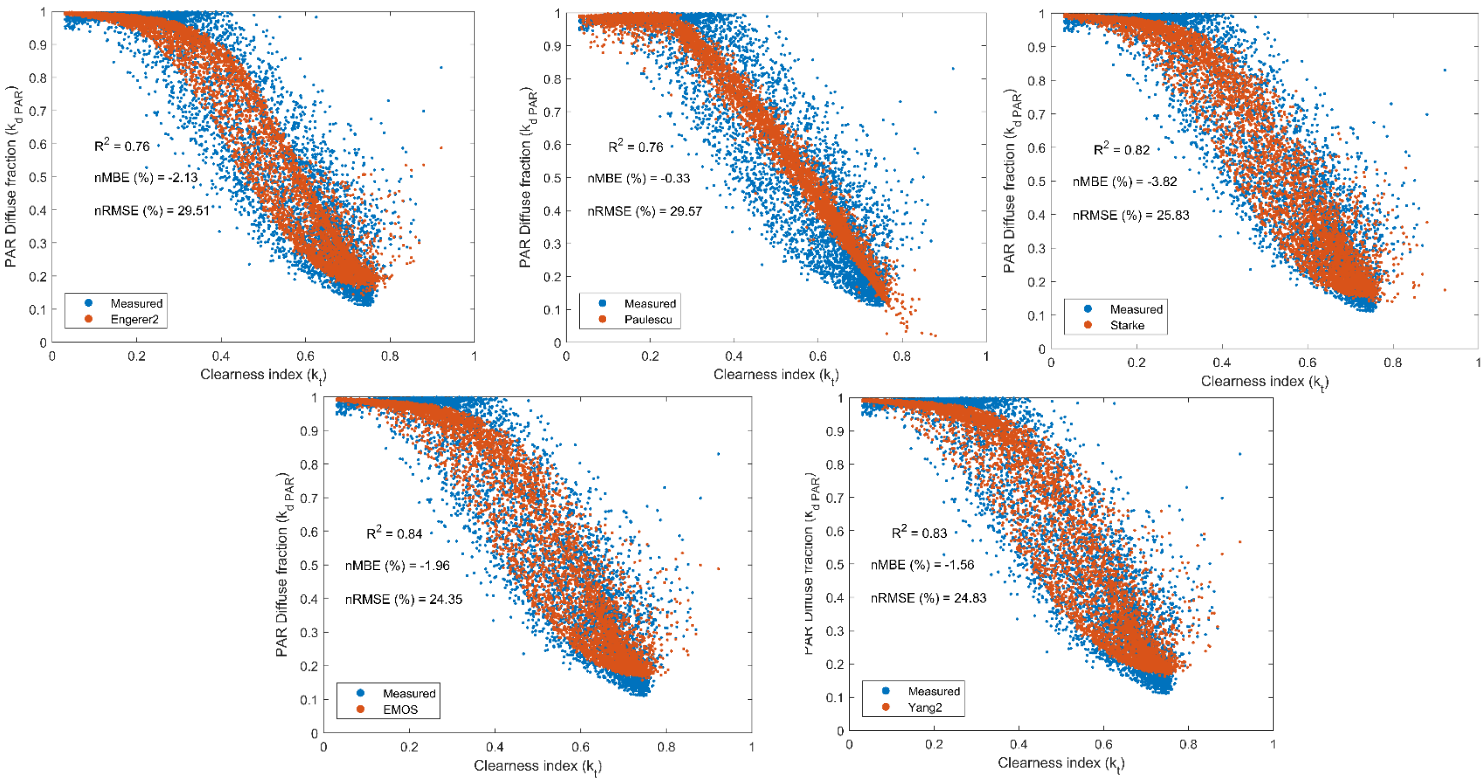

Figure 7. Diffuse PAR fraction data plotted against clearness index for the Hyltemossa station, overlaid with the results of 4 stand-alone and EMOS decomposition models using locally fitted coefficients (re-estimated). The total number of data points in each plot is the testing data sample listed in Table 2.

Table 6. Station-specific EMOS parameters estimated using 30-min data from ICOS-Sweden stations (Lanna 2017-2018, Hyltemossa 2015 and 2017, Norunda 2016-2017). Parameters $\hat{b}^{\text{GU}}, \cdots, \hat{b}^{\text{YANG2}}$ are the estimated mixing weights for the 6 component models respectively (using new fitted coefficients to the station locations), whereas $\hat{c}$ is the estimated amount of scaling for the ensemble variance.

Station	$\hat{b}^{\text{GU}}$	$\hat{b}^{\text{ABREU}}$	$\hat{b}^{\text{ENGERER2}}$	$\hat{b}^{\text{PAULESCU}}$	$\hat{b}^{\text{STARKE}}$	$\hat{b}^{\text{YANG2}}$	$\hat{c}$
Lanna	0.00	0.00	0.00	0.04	0.28	0.68	1.47
Hyltemossa	0.00	0.00	0.00	0.00	0.20	0.80	0.90
Norunda	0.00	0.00	0.00	0.02	0.26	0.72	1.13

Out of the six stand-alone models compared in this study, YANG2 is found to have the highest accuracy under squared error, both with original coefficients and locally fitted ones. This high accuracy can be directly associated to the satellite-derived diffuse fraction parameter characteristic of this model. As explained by Yang & Boland (2019) themselves, satellite-based irradiance estimates are usually based on physical models, hence, they are efficient and effective in explaining the low-frequency variability in diffuse irradiance component. Nevertheless, although satellite-augmented models are becoming more popular due to the worldwide availability of such data, there are still many locations where the resolution is not high enough, especially in high-latitude regions.

As for the study of an agrivoltaic site, if the objective is to evaluate the performance of a site when carrying out site selection feasibility study, it is most probably that previously collected irradiance data would be used as opposed to real-time data. Hence, no future values of clearness index would, in this case, be necessary to compute parameters such as daily clearness index. Consequently, STARKE model could be seen as an accurate model to be applied for PAR diffuse component prediction, with respect of YANG2 if satellite-derived data cannot be found.

Nonetheless, if there is data available that can satisfy all the inputs needed for the 6 stand-alone decomposition model in the selected location to build an agrivoltaic site, EMOS could be then applied to achieve further accuracy in estimating PAR diffuse component. To this extent, highest accuracy in predicting crop yield in the chosen site would be obtained, thus, bringing a better prognosis of the agrivoltaic site performance. Likewise, it is important to mention that in the present study, only six stand-alone models are chosen for testing the EMOS approach. However, other different decomposition models could be contemplated, and the number of models could also be re-considered, e.g., adding more than six models in the ensemble. Therefore, EMOS with a different selection of component models and number is object to further studies, as well as to reevaluate and include in the best model pool each time a new high-performance stand-alone decomposition model is suggested in the literature (Yang and Gueymard, 2020).

3.3. YANG2 and STARKE re-parameterized for Sweden

By thoroughly comparing the 6 stand-alone models and EMOS approach from the previous results section, and as one of the targets for this work, sets of coefficients for Sweden are proposed for the best performing stand-alone models: YANG2 as first, and STARKE as second. Explanation on why these two models are selected is made clear from the discussion presented above, the performance of the models is observable likewise in Table 5, thus, it will not be reiterated here again. The procedure in obtaining these coefficients is very similar to the one described in section 2.4. However, the training dataset in this case is the concatenation of the training data of the three locations (Lanna, Hyltemossa and Norunda) previously described in Table 2. The new sets of coefficients for YANG2 and STARKE for Sweden are shown in Table 7. With these new coefficients, the model is validated using the new testing data set, in this case, also concatenated from the testing data sets of the three locations studied. Results are shown in Figure 8. Error metrics with nRMSE of 25.56% for YANG2, 28.36% for STARKE and both models with R^2 above or equal to 0.8, present satisfactory accuracy results.

Table 7. Model coefficients of YANG2 and STARKE fitting using 2-year data of 3 locations in Sweden of 30-min data concatenated and collected at ICOS-Sweden stations (Lanna 2017-2018, Hyltemossa 2015 and 2017, Norunda 2016-2017).

YANG2	**STARKE**	
$C = 0.0888$	$\beta_0 = -4.4310$	$\beta_7 = -1.8476$
$\beta_0 = -2.6258$	$\beta_1 = 6.1760$	$\beta_8 = -0.2195$
$\beta_1 = 7.2506$	$\beta_2 = -0.0822$	$\beta_9 = -0.0287$
$\beta_2 = -0.0458$	$\beta_3 = 0.1358$	$\beta_{10} = -0.0204$
$\beta_3 = 0.0099$	$\beta_4 = 1.1433$	$\beta_{11} = 1.3971$
$\beta_4 = -0.0839$	$\beta_5 = 3.3757$	$\beta_{12} = 3.4869$
$\beta_5 = 0.5002$	$\beta_6 = -2.6396$	$\beta_{13} = 0.5026$
$\beta_6 = -2.1731$		

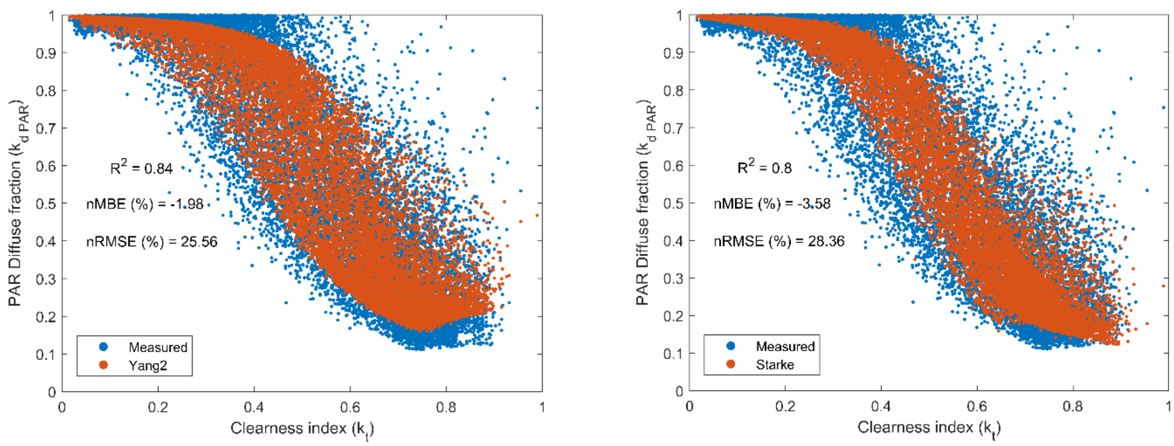

Figure 8. Diffuse PAR fraction data plotted against clearness index of the 3 stations in Sweden overlaid with the results of YANG2 (left) and STARKE (right) decomposition models. The total number of data points in each plot is the sum of the testing data for each location listed in Table 2.

4. Conclusions

A comparison of six stand-alone plus EMOS approach decomposition models for solar global radiation applied to PAR has been performed in this work. The three sites chosen for the validation of the models are in Sweden. Since none of the stand-alone models in their original publications had used data from the Scandinavian country to fit their parameters, the comparison was fair. Results by employing the original coefficients of the selected models showed that all the stand-alone models are not accurate when implemented in the selected Swedish locations due to general weak performances in terms of nRMSE ranging between 30-95%, except perhaps for YANG2 (29-34%).

In this context, re-parameterization of the models is highly recommended if measured data is available. Re-parameterization gave better accuracy performance for all the stand-alone models in the three studied locations in Sweden achieving nRMSE lowest as 24.31% and highest as 37.94%, improving therefore EMOS-based model as well (lowest nRMSE of 23.96%).

If satellite-derived irradiance data is accessible and resolution is deemed adequate, YANG2 is without doubt the best decomposition model up to date to be used to predict PAR diffuse component. Otherwise, STARKE is seen as the second-best performing model to be selected in no real-time predictions applications, for example, when evaluating potential sites for building agrivoltaic systems by using previously collected data.

EMOS can be applied in the event that wide amount of data is obtainable for a further accurate estimation of PAR diffuse component. To be noticed that EMOS parameters can also be fitted using other techniques and it is important to keep in mind that the performance of EMOS-based model depends on the accuracies of the decomposition models forming the ensemble.

The sets of coefficients determined for Sweden in this study for the best-performing models, YANG2 and STARKE, can be applied to obtain an accurate first estimation of the amount of PAR diffuse component reaching the crops when evaluating site-selection of agrivoltaic systems. Site specific coefficients can be computed afterwards if measurements are available during the operation of the agrivoltaic system to have an even superior assessment of PAR and subsequently of crop yield.

The overall methodology applied in this work for Sweden can be similarly executed for other countries.

Acknowledgements

The authors acknowledge the financial support received from the Swedish Energy Agency through the project "Evaluation of the first agrivoltaic system in Sweden", grant number 51000-1. The authors also acknowledge the funding received from the Swedish Energy Agency through the project SOLVE, grant number 52693-1. Lastly, author Pietro Elia Campana acknowledges Formas - a Swedish Research Council for Sustainable Development, for the funding received through the early career project “Avoiding conflicts between the sustainable development goals through agro-photovoltaic systems”, grant number FR-2021/0005.

Likewise, the authors acknowledge ICOS Sweden for provisioning of Lanna, Hyltemossa and Norunda stations data. ICOS Sweden is funded by the Swedish Research Council as a national research infrastructure.

References

Abreu, E.F.M., Canhoto, P., Costa, M.J., 2019. Prediction of diffuse horizontal irradiance using a new climate zone model. Renew. Sustain. Energy Rev. 110, 28–42. https://doi.org/10.1016/j.rser.2019.04.055

Alton, P.B., 2008. Reduced carbon sequestration in terrestrial ecosystems under overcast skies compared to clear skies. Agric. For. Meteorol. 148, 1641–1653. https://doi.org/10.1016/j.agrformet.2008.05.014

Benedetti, M., Vecchi, V., Barera, S., Dall'Osto, L., 2018. Biomass from microalgae: the potential of domestication towards sustainable biofactories. Microb. Cell Factories 17, 173. https://doi.org/10.1186/s12934-018-1019-3

Bird, R.E., Riordan, C., 1986. Simple Solar Spectral Model for Direct and Diffuse Irradiance on Horizontal and Tilted Planes at the Earth's Surface for Cloudless Atmospheres. J. Clim. Appl. Meteorol. 25, 87–97. https://doi.org/10.1175/1520-0450(1986)025<0087:SSSMFD>2.0.CO;2

Bright, J.M., Engerer, N.A., 2019. Engerer2: Global re-parameterisation, update, and validation of an irradiance separation model at different temporal resolutions. J. Renew. Sustain. Energy 11, 033701. https://doi.org/10.1063/1.5097014

Campana, P.E., Stridh, B., Amaducci, S., Colauzzi, M., 2021. Optimisation of vertically mounted agrivoltaic systems. J. Clean. Prod. 325, 129091. https://doi.org/10.1016/j.jclepro.2021.129091

CAMS radiation service [WWW Document], 2021. . SoDa. URL http://www.soda-pro.com/web-services/radiation/cams-radiation-service (accessed 12.6.21).

Cebula, R.P., Thuillier, G.O., VanHoosier, M.E., Hilsenrath, E., Herse, M., Brueckner, G.E., Simon, P.C., 1996. Observations of the solar irradiance in the 200-350 nm interval during the ATLAS-1 Mission: A comparison among three sets of measurements-SSBUV, SOLSPEC, and SUSIM. Geophys. Res. Lett. 23, 2289–2292. https://doi.org/10.1029/96GL01109

Cheng, S.J., Bohrer, G., Steiner, A.L., Hollinger, D.Y., Suyker, A., Phillips, R.P., Nadelhoffer, K.J., 2015. Variations in the influence of diffuse light on gross primary productivity in temperate ecosystems. Agric. For. Meteorol. 201, 98–110. https://doi.org/10.1016/j.agrformet.2014.11.002

Cruse, M.J., Kucharik, C.J., Norman, J.M., 2015. Using a Simple Apparatus to Measure Direct and Diffuse Photosynthetically Active Radiation at Remote Locations. PLOS ONE 10, e0115633. https://doi.org/10.1371/journal.pone.0115633

Delta T, 2022. BF5 Sunshine Sensor - Pyranometer - Solar Radiation [WWW Document]. Delta T. URL https://delta-t.co.uk/product/bf5/ (accessed 2.2.22).

Duffie, J.A., Beckman, W.A., 2013. Solar engineering of thermal processes / John A. Duffie, William A. Beckman, 4th ed. ed. John Wiley, Hoboken.

Engerer, N.A., 2015. Minute resolution estimates of the diffuse fraction of global irradiance for southeastern Australia. Sol. Energy 116, 215–237. https://doi.org/10.1016/j.solener.2015.04.012

Evaluation of the first agrivoltaic system in Sweden – Mälardalens universitet [WWW Document], 2022. URL https://www.mdh.se/en/malardalen-university/research/research-projects/evaluation-of-the-first-agrivoltaic-system-in-sweden (accessed 1.26.22).

Ferrera-Cobos, F., Vindel, J.M., Valenzuela, R.X., González, J.A., 2020. Analysis of Spatial and Temporal Variability of the PAR/GHI Ratio and PAR Modeling Based on Two Satellite Estimates. Remote Sens. 12, 1262. https://doi.org/10.3390/rs12081262

Ferro, L., 2019. Wastewater treatment and biomass generation by Nordic microalgae Growth in subarctic climate and microbial interactions.

Gneiting, T., Raftery, A.E., Westveld, A.H., Goldman, T., 2005. Calibrated Probabilistic Forecasting Using Ensemble Model Output Statistics and Minimum CRPS Estimation. Mon. Weather Rev. 133, 1098–1118. https://doi.org/10.1175/MWR2904.1

Goudriaan, J., Van Laar, H.H., 1994. Modelling Potential Crop Growth Processes, Current Issues in Production Ecology. Springer Netherlands, Dordrecht. https://doi.org/10.1007/978-94-011-0750-1

Gschwind, B., Wald, L., Blanc, P., Lefèvre, M., Schroedter-Homscheidt, M., Arola, A., 2019. Improving the McClear model estimating the downwelling solar radiation at ground level in cloud-free conditions – McClear-v3. Meteorol. Z. 28, 147–163. https://doi.org/10.1127/metz/2019/0946

Gu, L., Baldocchi, D., Verma, S.B., Black, T.A., Vesala, T., Falge, E.M., Dowty, P.R., 2002. Advantages of diffuse radiation for terrestrial ecosystem productivity. J. Geophys. Res. Atmospheres 107, ACL 2-1-ACL 2-23. https://doi.org/10.1029/2001JD001242

Gu, L., Baldocchi, D.D., Wofsy, S.C., Munger, J.W., Michalsky, J.J., Urbanski, S.P., Boden, T.A., 2003. Response of a Deciduous Forest to the Mount Pinatubo Eruption: Enhanced Photosynthesis. Science 299, 2035–2038. https://doi.org/10.1126/science.1078366

Gu, L., Fuentes, J.D., Shugart, H.H., Staebler, R.M., Black, T.A., 1999. Responses of net ecosystem exchanges of carbon dioxide to changes in cloudiness: Results from two North American deciduous forests. J. Geophys. Res. Atmospheres 104, 31421–31434. https://doi.org/10.1029/1999JD901068

Gueymard, C., 1995. Simple Model for the Atmospheric Radiative Transfer of Sunshine (SMARTS2) Algorithms and performance assessment 84.

Gueymard, C.A., 2018. A reevaluation of the solar constant based on a 42-year total solar irradiance time series and a reconciliation of spaceborne observations. Sol. Energy 168, 2–9. https://doi.org/10.1016/j.solener.2018.04.001

Gueymard, C.A., 2004. The sun’s total and spectral irradiance for solar energy applications and solar radiation models. Sol. Energy 76, 423–453. https://doi.org/10.1016/j.solener.2003.08.039

Gueymard, C.A., Ruiz-Arias, J.A., 2016. Extensive worldwide validation and climate sensitivity analysis of direct irradiance predictions from 1-min global irradiance. Sol. Energy 128, 1–30. https://doi.org/10.1016/j.solener.2015.10.010

Hu, B., Wang, Y., Liu, G., 2007. Spatiotemporal characteristics of photosynthetically active radiation in China. J. Geophys. Res. 112, D14106. https://doi.org/10.1029/2006JD007965

ICOS Sweden [WWW Document], 2021. URL https://www.icos-sweden.se/ (accessed 12.6.21).

Jacovides, C.P., Boland, J., Asimakopoulos, D.N., Kaltsounides, N.A., 2010. Comparing diffuse radiation models with one predictor for partitioning incident PAR radiation into its diffuse component in the eastern Mediterranean basin. Renew. Energy 35, 1820–1827. https://doi.org/10.1016/j.renene.2009.11.015

Jacovides, C.P., Tymvios, F.S., Asimakopoulos, D.N., Theofilou, K.M., Pashiardes, S., 2003. Global photosynthetically active radiation and its relationship with global solar radiation in the Eastern Mediterranean basin. Theor. Appl. Climatol. 74, 227–233. https://doi.org/10.1007/s00704-002-0685-5

Kathilankal, J.C., O’Halloran, T.L., Schmidt, A., Hanson, C.V., Law, B.E., 2014. Development of a semi-parametric PAR (Photosynthetically Active Radiation) partitioning model for the United States, version 1.0. Geosci. Model Dev. 7, 2477–2484. https://doi.org/10.5194/gmd-7-2477-2014

Keppel-Aleks, G., Washenfelder, R.A., 2016. The effect of atmospheric sulfate reductions on diffuse radiation and photosynthesis in the United States during 1995-2013: Effect of SO_2 Reductions on Photosynthesis. Geophys. Res. Lett. 43, 9984–9993. https://doi.org/10.1002/2016GL070052

Knohl, A., Baldocchi, D.D., 2008. Effects of diffuse radiation on canopy gas exchange processes in a forest ecosystem: DIFFUSE RADIATION EFFECTS IN FOREST. J. Geophys. Res. Biogeosciences 113, n/a-n/a. https://doi.org/10.1029/2007JG000663

Koblick, D., 2021. Vectorized Solar Azimuth and Elevation Estimation [WWW Document]. MATLAB Cent. File Exch. URL https://se.mathworks.com/matlabcentral/fileexchange/23051-vectorized-solar-azimuth-and-elevation-estimation (accessed 12.9.21).

Kottek, M., Grieser, J., Beck, C., Rudolf, B., Rubel, F., 2006. World Map of the Köppen-Geiger climate classification updated. Meteorol. Z. 15, 259–263. https://doi.org/10.1127/0941-2948/2006/0130

Laccio, D., Alonso-Suárez, R., Abal, G., 2021. ONE-MINUTE ASSESSMENT OF PHOTOSYNTHETICALLY ACTIVE RADIATION (PAR) MODELS IN URUGUAY.

Langhans, R.W., Tibbitts, T.W., Use, N.C.R.C.N.-101 on C.E.T. and, 1997. Plant Growth Chamber Handbook. Iowa Agricultural and Home Economics Experiment Station.

Lefèvre, M., Oumbe, A., Blanc, P., Espinar, B., Gschwind, B., Qu, Z., Wald, L., Schroedter-Homscheidt, M., Hoyer-Klick, C., Arola, A., Benedetti, A., Kaiser, J.W., Morcrette, J.-J., 2013. McClear: a new model estimating downwelling solar radiation at ground level in clear-sky conditions. Atmospheric Meas. Tech. 6, 2403–2418. https://doi.org/10.5194/amt-6-2403-2013

Leuning, R., Kelliher, F.M., Pury, D.G.G., Schulze, E.-D., 1995. Leaf nitrogen, photosynthesis, conductance and transpiration: scaling from leaves to canopies. Plant Cell Environ. 18, 1183–1200. https://doi.org/10.1111/j.1365-3040.1995.tb00628.x

Liu, B.Y.H., Jordan, R.C., 1960. The interrelationship and characteristic distribution of direct, diffuse and total solar radiation. Sol. Energy 4, 1–19. https://doi.org/10.1016/0038-092X(60)90062-1

MathWorks [WWW Document], 2021. URL https://se.mathworks.com/help/optim/ug/fmincon.html (accessed 12.6.21).

McCree, K.J., 1972. Test of current definitions of photosynthetically active radiation against leaf photosynthesis data. Agric. Meteorol. 10, 443–453. https://doi.org/10.1016/0002-1571(72)90045-3

McCree, K.J., 1971. The action spectrum, absorptance and quantum yield of photosynthesis in crop plants. Agric. Meteorol. 9, 191–216. https://doi.org/10.1016/0002-1571(71)90022-7

Mercado, L.M., Bellouin, N., Sitch, S., Boucher, O., Huntingford, C., Wild, M., Cox, P.M., 2009. Impact of changes in diffuse radiation on the global land carbon sink. Nature 458, 1014–1017. https://doi.org/10.1038/nature07949

Misson, L., Lunden, M., McKay, M., Goldstein, A.H., 2005. Atmospheric aerosol light scattering and surface wetness influence the diurnal pattern of net ecosystem exchange in a semi-arid ponderosa pine plantation. Agric. For. Meteorol. 129, 69–83. https://doi.org/10.1016/j.agrformet.2004.11.008

Mõttus, M., Sulev, M., Frederic, B., Lopez-Lozano, R., Noorma, A., 2011. Photosynthetically Active Radiation: Measurement and Modeling, in: Encyclopedia of Sustainability Science and Technology. pp. 7970–8000.

Mousavi Maleki, S., Hizam, H., Gomes, C., 2017. Estimation of Hourly, Daily and Monthly Global Solar Radiation on Inclined Surfaces: Models Re-Visited. Energies 10, 134. https://doi.org/10.3390/en10010134

Noriega Gardea, M.M.A., Corral Martínez, L.F., Anguiano Morales, M., Trujillo Schiaffino, G., Salas Peimbert, D.P., 2020. MODELLING PHOTOSYNTHETICALLY ACTIVE RADIATION: A REVIEW. Atmósfera. https://doi.org/10.20937/ATM.52737

Norman, J.M., Welles, J.M., 1983. Radiative Transfer in an Array of Canopies. Agron. J. 75, 481–488. https://doi.org/10.2134/agronj1983.00021962007500030016x

Nwokolo, S., 2018. A Global Review of Empirical Models for Estimating Photosynthetically Active Radiation. Trends Renew. Energy 4. https://doi.org/10.17737/tre.2018.4.2.0079

Oliphant, A.J., Dragoni, D., Deng, B., Grimmond, C.S.B., Schmid, H.-P., Scott, S.L., 2011. The role of sky conditions on gross primary production in a mixed deciduous forest. Agric. For. Meteorol. 151, 781–791. https://doi.org/10.1016/j.agrformet.2011.01.005

Oliphant, A.J., Stoy, P.C., 2018. An Evaluation of Semiempirical Models for Partitioning Photosynthetically Active Radiation Into Diffuse and Direct Beam Components. J. Geophys. Res. Biogeosciences 123, 889–901. https://doi.org/10.1002/2017JG004370

Paulescu, E., Blaga, R., 2016. Regression models for hourly diffuse solar radiation. Sol. Energy 125, 111–124. https://doi.org/10.1016/j.solener.2015.11.044

Qu, Z., Oumbe, A., Blanc, P., Espinar, B., Gesell, G., Gschwind, B., Klüser, L., Lefèvre, M., Saboret, L., Schroedter-Homscheidt, M., Wald, L., 2017. Fast radiative transfer parameterisation for assessing the surface solar irradiance: The Heliosat-4 method. Meteorol. Z. 26, 33–57. https://doi.org/10.1127/metz/2016/0781

Reindl, D.T., Beckman, W.A., Duffie, J.A., 1990. Diffuse fraction correlations. Sol. Energy 45, 1–7. https://doi.org/10.1016/0038-092X(90)90060-P

Ren, X., He, H., Zhang, L., Yu, G., 2018. Global radiation, photosynthetically active radiation, and the diffuse component dataset of China, 1981–2010. Earth Syst. Sci. Data 10, 1217–1226. https://doi.org/10.5194/essd-10-1217-2018

Ren, X., He, H., Zhang, L., Yu, G., 2014. Estimation of diffuse photosynthetically active radiation and the spatiotemporal variation analysis in China from 1981 to 2010. J. Geogr. Sci. 24, 579–592. https://doi.org/10.1007/s11442-014-1107-1

Robledo, L., Soler, A., 2000. Luminous efficacy of global solar radiation for clear skies. Energy Convers. Manag. 41, 1769–1779. https://doi.org/10.1016/S0196-8904(00)00019-4

Rubel, F., Brugger, K., Haslinger, K., Auer, I., 2017. The climate of the European Alps: Shift of very high resolution Köppen-Geiger climate zones 1800–2100. Meteorol. Z. 26, 115–125. https://doi.org/10.1127/metz/2016/0816

S, P., Sa, K., A, P., 2017. Characteristics of Photosynthetic Active Radiation (PAR) Through Statistical Analysis at Larnaca, Cyprus. SM J. Biom. Biostat. 2, 1–16. https://doi.org/10.36876/smjbb.1009

Smith, ElskeV.P., Gottlieb, DavidM., 1974. Solar flux and its variations. Space Sci. Rev. 16. https://doi.org/10.1007/BF00182600

Spencer, J. W, 1971. Fourier Series Representation of the Position of the Sun. Search 2, 172.

Spitters, C.J.T., Toussaint, H.A.J.M., Goudriaan, J., 1986. Separating the diffuse and direct component of global radiation and its implications for modeling canopy photosynthesis Part I. Components of incoming radiation. Agric. For. Meteorol. 38, 217–229. https://doi.org/10.1016/0168-1923(86)90060-2

Starke, A.R., Lemos, L.F.L., Boland, J., Cardemil, J.M., Colle, S., 2018. Resolution of the cloud enhancement problem for one-minute diffuse radiation prediction. Renew. Energy 125, 472–484. https://doi.org/10.1016/j.renene.2018.02.107

Still, C.J., Riley, W.J., Biraud, S.C., Noone, D.C., Buenning, N.H., Randerson, J.T., Torn, M.S., Welker, J., White, J.W.C., Vachon, R., Farquhar, G.D., Berry, J.A., 2009. Influence of clouds and diffuse radiation on ecosystem-atmosphere CO_2 and $CO^{18}O$ exchanges. J. Geophys. Res. 114, G01018. https://doi.org/10.1029/2007JG000675

Tsubo, M., Walker, S., 2005. Relationships between photosynthetically active radiation and clearness index at Bloemfontein, South Africa. Theor. Appl. Climatol. 80, 17–25. https://doi.org/10.1007/s00704-004-0080-5

US Department of Commerce, N., 2021. ESRL Global Monitoring Laboratory - Global Radiation and Aerosols [WWW Document]. URL https://gml.noaa.gov/grad/solcalc/calcdetails.html (accessed 12.14.21).

Wang, Q., Tenhunen, J., Schmidt, M., Kolcun, O., Droesler, M., Reichstein, M., 2006. Estimation of total, direct and diffuse PAR under clear skies in complex alpine terrain of the National Park Berchtesgaden, Germany. Ecol. Model. 196, 149–162. https://doi.org/10.1016/j.ecolmodel.2006.02.005

Weiss, A., Norman, J.M., 1985. Partitioning solar radiation into direct and diffuse, visible and near-infrared components. Agric. For. Meteorol. 34, 205–213. https://doi.org/10.1016/0168-1923(85)90020-6

Wood, J., Muneer, T., Kubie, J., 2003. Evaluation of a New Photodiode Sensor for Measuring Global and Diffuse Irradiance, and Sunshine Duration. J. Sol. Energy Eng. 125, 43–48. https://doi.org/10.1115/1.1531149

Xia, X., Li, Z., Wang, P., Cribb, M., Chen, H., Zhao, Y., 2008. Analysis of photosynthetic photon flux density and its parameterization in Northern China. Agric. For. Meteorol. 148, 1101–1108. https://doi.org/10.1016/j.agrformet.2008.02.008

Yang, D., Boland, J., 2019. Satellite-augmented diffuse solar radiation separation models. J. Renew. Sustain. Energy 11, 023705. https://doi.org/10.1063/1.5087463

Yang, D., Gueymard, C.A., 2020. Ensemble model output statistics for the separation of direct and diffuse components from 1-min global irradiance. Sol. Energy 208, 591–603. https://doi.org/10.1016/j.solener.2020.05.082

Yu, X., Guo, X., 2016. Hourly photosynthetically active radiation estimation in Midwestern United States from artificial neural networks and conventional regressions models. Int. J. Biometeorol. 60, 1247–1259. https://doi.org/10.1007/s00484-015-1120-9